MM-WAVE CONFOCAL RESONATORS FOR VERTICAL STRUCTURE PROFILING IN SEMICONDUCTING AND SUPERCONDUCTING MATERIALS

J. S. Martens, L. Lee, K. Char, R. Withers, and D. Zhang
Conductus, Inc.
Sunnyvale, CA

V. M. Hietala, C. P. Tigges, and J. Zolper
Sandia National Laboratories
Albuquerque, NM

ABSTRACT

The confocal resonator is a tool for quick, accurate, non-invasive and flexible surface impedance measurements. From the frequency dependence of surface impedance, the vertical conductivity/permittivity profiles have been determined for a variety of devices and device materials including implanted Si and GaAs wafers and superconductor-dielectric interfaces. The vertical spatial resolution can be as small as several nm and accuracy of the complex permittivity generally is better than 3 %.

INTRODUCTION

Confocal resonant structures [1] have been used to evaluate dielectrics and surface resistance properties and to image surface impedance over a large lateral area [2-4]. This open resonant structure is useful because of its sensitivity, non-invasiveness and scalability (in terms of frequency and sample size). Another measurement of interest is the vertical profile, in terms of complex conductivity/permittivity, that can be extracted from the frequency dependence of the surface impedance. Of relevance are the vertical resolution, the types of materials/structures that can be analyzed and the accuracy of the computed complex permittivity/conductivity for each of these material types. These characteristics of the measurement tool will be studied in the context of a number of experiments designed to illustrate a subset of presently interesting measurements in the semiconductor and superconductor fields.

THE TECHNIQUE

The usual confocal resonator structure is shown in Fig. 1. A spherical mirror of radius of curvature b is placed a distance $b/2$ above the sample under test. A well-known Gaussian wave solution exists in the structure with the resonant mode of interest being TEM_{00n}[1]. The resonant condition is met when $bk=\pi(2n+1)/2$ (where $k=\omega/c$, n even) resulting in a mode spacing (for a fixed mirror-sample spacing) of a few GHz for most mirror sizes and for mm-wave frequencies. A single mirror can be used over at least a waveguide band with a reasonable spot size, coupling and diffraction losses. For hardware reasons and the desire to keep diffraction losses low, several mirrors are used to cover the desired broad frequency range although this will probably not be done in the future. Presently 30-170 GHz is used although greater bandwidth will improve resolution. The radius of curvature ranges from 4-10 cm for the mirrors used and all have been made from aluminum with a nominal surface resistance of 100-300 mΩ at 94 GHz and 300K. All of the mirror-sample cavities are coupled to a rectangular waveguide feed through a circular aperture. The reflectometry is done with commercial network analyzers below 40 GHz and with conventional assemblies of couplers, isolators, detectors and swept Gunn sources (multiplied for frequencies above 100 GHz) above 40 GHz. Resolution is about 1 mΩ at 94 GHz and scales roughly as $\omega^{0.5}$ for other frequencies in this range.

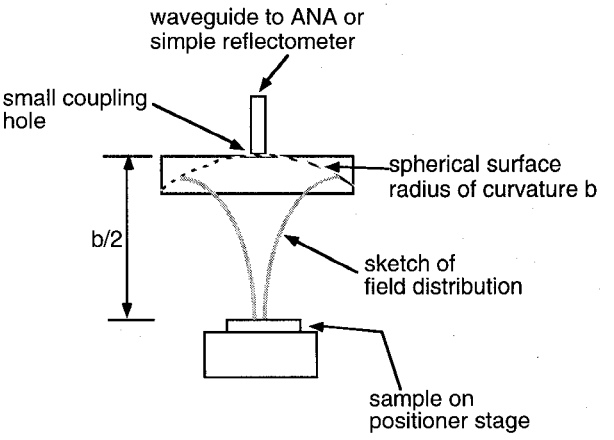

Figure 1. Basic structure of the confocal resonator. Commercial network analyzers are used at lower frequencies and simple reflectometers are used above 40 GHz (several mirrors are used).

It is easy to see that since the skin depth varies with frequency, the portion of the material being probed for surface impedance will vary with frequency. If the field distribution can be properly deconvolved from the data, the vertical distribution of the complex conductivity/permittivity can be extracted. The problem will be analyzed as a non-uniform transmission line [5-6]. The plane wave (in the TEM_{00n} mode), incident on the sample, enters a region where both wave impedance and propagation coefficients vary with vertical position z (neglecting lateral variations). Using standard incremental reflection arguments [5], which must be generalized to allow larger slews in material properties, it is then possible to arrive at an analytic relationship between a given material profile and the input reflection coefficient which is directly extracted from surface impedance measurements.

CH3277-1/93/0000-1243$01.00 © 1993 IEEE

From the Q_0 (the uncoupled quality factor extracted from conventional 1 port resonator techniques) and frequency of the resonance, the real part of the surface impedance R_s can be easily determined with high accuracy. The relevant equation is

$$R_{ss} = \frac{\omega_0 \mu_0 b}{4Q_0} - R_{sm} \tag{1}$$

where R_{ss} is the surface resistance of the sample at a resonant frequency ω_0 (many are used during the measurement) and R_{sm} is the surface resistance of the mirror (determined by calibration and shown to be stable).

The imaginary part of the surface impedance is determined through the resonant frequency. Reference resonant frequencies are obtained from a test pattern on or near the top of the actual sample (usually co-evaporated). From this data and the measured resonant frequencies on the sample proper, the actual imaginary part of surface impedance as a function of frequency can be extracted as shown in Eq. 2.

$$X_{s,sample} = X_{s,cal} - \frac{\mu_0 b}{2}\left(\omega_{0,sample} - \omega_{0,cal}\right) \tag{2}$$

where $X_{s,cal}$ and $\omega_{0,cal}$ are the surface reactance and resonant frequency, respectively, corresponding to the calibration surface (typically Ag). $X_{s,sample}$ and $\omega_{0,sample}$ are the surface reactance and resonant frequency, respectively, of the sample under test.

From the surface impedance data, it is straightforward to calculate the reflection coefficient of the sample (in a free space sense). This is the data needed to apply the non-uniform transmission line analysis. For non-magnetic materials, the relationship between the reflection coefficient $\Gamma(\omega)$ and the complex permittivity $\hat{\varepsilon}(z)$ is given by

$$\Gamma(\omega) = -\frac{1}{2}\int_0^L \left\{ e^{-2\int_0^z \gamma(x)dx} \frac{d}{dz}\left[\ln(\overline{\eta})\right] \right\} dz$$

$$\gamma(z) = \omega\sqrt{\mu_0 \hat{\varepsilon}(z)} \tag{3}$$

$$\overline{\eta}(z) = \sqrt{\frac{\varepsilon_0}{\hat{\varepsilon}(z)}}$$

Here γ is the complex propagation constant and $\overline{\eta}$ is the wave impedance normalized to free space. The complex permittivity $\hat{\varepsilon}(z)$ is treated here in the generalized sense in that conduction, polarization and other losses can all be included in Im{ $\hat{\varepsilon}(z)$ }.

From the measured $\Gamma(\omega)$, we invert the integral equation (first line of Eq. 3) which in general will not produce a unique solution. The constraint of physical realizability of the materials does help considerably. As an example, when the material region is a lossy dielectric the frequency dependence of the complex permittivity is relatively well-defined. If the material is a simple conductor, the real part of conductivity ($\omega\varepsilon''$ in this simple model) will be independent of frequency. Similar assumptions can be made for a variety of materials allowing for numerically efficient processing of Eq. 3 which is generally done in a least squares fashion.

These assumptions allow at least a piecewise approximation of the solution to be found. In other cases where additional information is available, more precise profiles can be extracted. As an example, in the case of a doped semiconductor wafer, the $\sigma(z)$ distribution (easily related to the permittivity function in eq. 3) is generally assumed to be a real combination of Gaussians, exponentials and discrete delta functions (requiring a partitioning of the summation of reflections) to accommodate a wide variety of doping profiles. This reduces computation time dramatically but can be generalized (including imaginary components for more lightly doped samples) as the problem warrants. In many thin film growth problems, the structure can be considered as simple finite layers (including interface zones) thus providing a physically meaningful, but finite, set of variables.

DATA AND ANALYSIS

As a first demonstration of the technique, a commercial GaAs wafer with peak doping at a depth of about 700 nm was measured (using a bandwidth of 75 GHz). The profile extracted from the confocal data is shown in Fig. 2 along with that measured by Secondary Ion Mass Spectroscopy (SIMS), a destructive technique, of a sample from the same wafer. A profile of the form

$$\sigma(z) = A + Be^{-\frac{(z-C)^2}{D}} + Ee^{-\frac{|z-F|}{G}} \tag{4}$$

was assumed for simplicity and was found to work adequately since the doping levels (both peak and background) were relatively high.

In addition, a simpler, doped Si wafer was tested. The confocal-derived profile was nearly Gaussian. The measured reflection coefficient data is shown in Fig. 3 along with the fit (simulated Γ) that corresponds to the expected distribution (peak doping of 4 10^{16} cm^{-3} at 1.5 μm below the surface). To illustrate the sensitivity of the technique, the simulated reflection coefficient data for a peak of 4 10^{16} cm^{-3} at 1.4 μm is also shown. Since changes of 0.01 in reflection coefficient are quite easily detected, the technique is sensitive to differences of this magnitude.

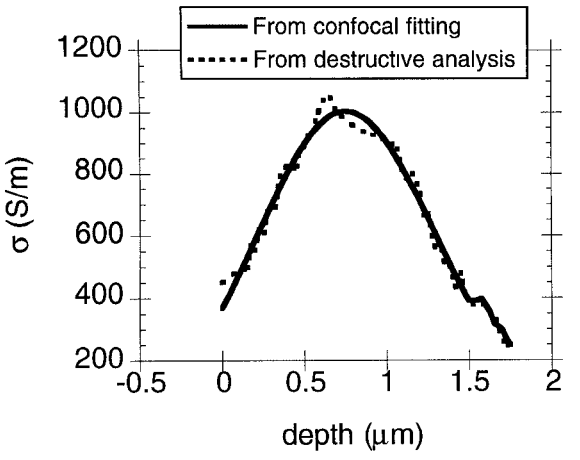

Figure 2. Conductivity profile in a GaAs wafer fit from confocal data and expected from SIMS analysis. The tail (non-Gaussian) on the inside edge of the distribution was successfully detected. It is believed that the difference at the peak is due to slight differences between the test samples.

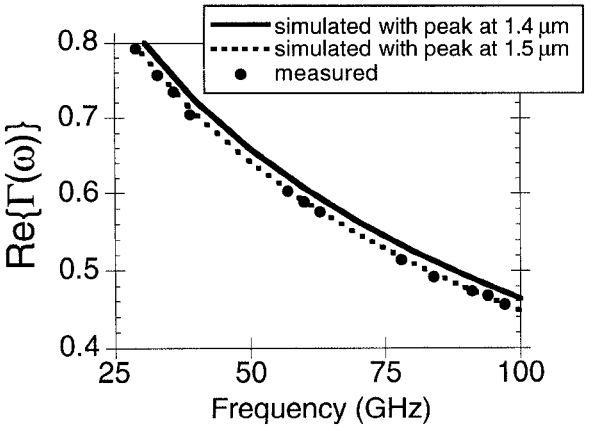

Figure 3. Plot of measured and simulated real part of reflection coefficient from an implanted Si wafer. The plot is to illustrate the quality of fit with the simulations and show the sensitivity of the technique to different profiles.

A third semiconductor example (Si) was also tested to illustrate the probing of ultrashallow doping profiles. The carrier concentration as a function of depth is shown in Fig. 4 from confocal results and from destructive SIMS analysis. Even at the depth scale of tens of nm, the confocal resonator approach was able to extract a doping profile that agrees reasonably well with that found from SIMS analysis of a companion sample. The differences at the surface and deep in the sample are believed to be due to the fact that the confocal resonator approach only detects activated carriers (which makes the technique ideal for the study of Schottky barriers and other devices). It is believed that dopants deep in the sample are not activated during the rapid thermal anneal that this sample experienced. The surface may not be entirely activated due to depletion resulting from band bending.

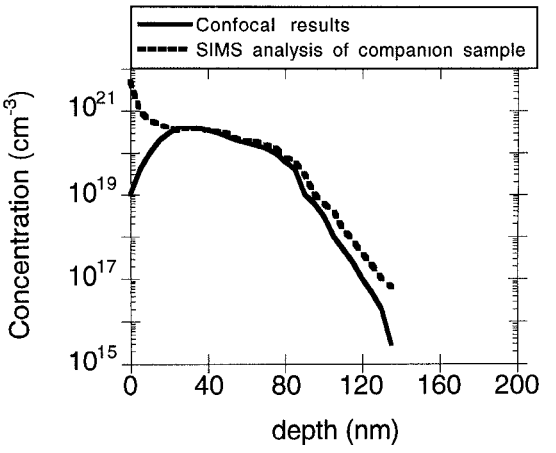

Figure 4. Dopant profile of an ultrashallow implant together with the SIMS result. Some of the discrepancy is due to the fact that the confocal analysis method only detects activated carriers.

The interface between a high temperature superconducting (HTS) film, YBaCuO, and its substrate, $LaAlO_3$, was also investigated. This experiment illustrates the variety of materials with which the approach is compatible and addresses an issue of fundamental technical concern for HTS circuit manufacturing. The structure of two samples, one having good, uniform transport properties and one having poor transport behavior, are shown in Fig. 5. As expected, the interface is quite clean on film A indicating only a few monolayers of disruption. The structure of film B is far more complicated, possibly a result of considerable interdiffusion between the substrate and the HTS film.

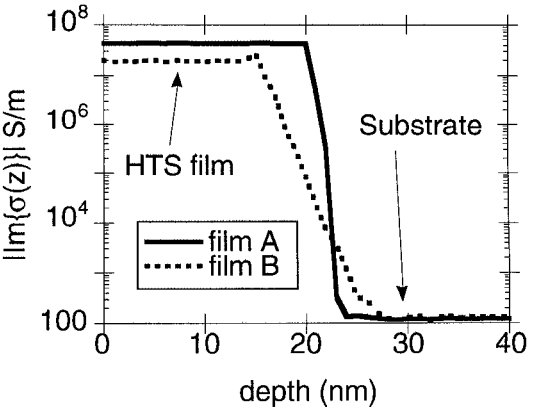

Figure 5. Profile of $|\mathrm{Im}\{\sigma(z)\}|$ for two YBaCuO films grown on $LaAlO_3$ (both nominally 20-25 nm thick) at 77K. Film A was of high quality based on transport measurements while film B showed poor performance. The ill-defined transition region in film B suggests interdiffusion.

A more complicated layered structure was considered next. This sample consists of a Au top level, a $SrTiO_3$ dielectric layer and a YBaCuO superconducting bottom layer. The top two layers are nominally 200 and 300 nm thick respectively and the YBaCuO layer is at least 300 nm thick. A plot of $|\mathrm{Im}\{\sigma(z)\}|$ is shown in Fig. 6. Note the broad transition to the YBaCuO layer and the presence of dielectric defects. The value of $|\mathrm{Im}\{\sigma\}|$ is very high in the dielectric as is consistent with the large dielectric constant of $SrTiO_3$. It is ,however, more than a factor of 2 smaller than bulk values as is common for $SrTiO_3$ thin films. The difference between 77K and 300K normal metal results is as expected and the difference for the superconducting layer is substantial. This is also expected [8] and the very low 300K value is consistent with the low carrier densities seen in the HTS materials in the normal state.

EXPECTATIONS/LIMITATIONS OF THE TECHNIQUE

The vertical resolution and accuracy is dependent on the material properties. For heavily doped semiconductors, the total accessible depth is a few microns while for superconductors, 500 nm is a practical limit. Thicker samples of lightly doped semiconductors may be analyzed providing a conducting back plane is available (to ensure a resonance) and the density of scattering objects is not too high. Features as thin as 1 nm can be detected as long as the deviation in conductivity from that of the surrounding material is large. As an example, a 10^{11} cm^{-2} 2DEG layer in a background of 10^{17} cm^{-3} can almost always be detected and its thickness can be calculated if it is larger than about 10 nm.

The accuracy in terms of the materials properties is dependent on the other materials present in the system. In the case of a simple multilevel dielectric problem (low loss with some reflector behind the dielectrics), the dielectric constant can be extracted to within about 1% and the loss tangent to within about $\pm 10^{-5}$. In the case of a lossy dielectric problem (such as lightly- to moderately-doped semiconductors), the real and imaginary parts of permittivity can each be extracted to within 2-5% (the lower limit on the imaginary part occurs as described above). In the case of a conductor problem, a more highly-doped semiconductor for example, the real part of conductivity (and hence doping density) can be extracted to within about 2% and the imaginary part of conductivity to within about 10%.

This approach offers a number of advantages over competing techniques. It is clearly non-invasive, does not require sample contact and can work with active areas as small as 0.1 mm^2. This gives the approach significant advantages over SIMS and other surface analytic techniques [7]. The range of depth that can be profiled is from 1 to 100s of microns depending on the local conductivity which gives it more depth flexibility than most optical techniques. The dynamic range in terms of conductivities is also much larger than with optical techniques: from the insulating state to over 10^{21} cm^{-3}. Conversely, the range of loss tangents of dielectrics that can be measured ranges from 10^{-5} to 1 (a normal conductor) assuming that the sample structure is appropriate.

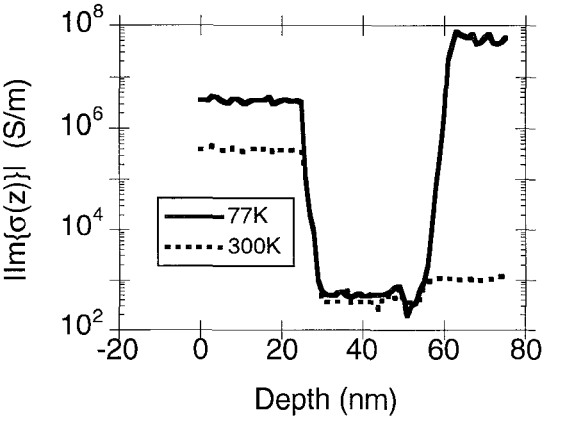

Figure 6. Plot of $|\mathrm{Im}\{\sigma\}|$ as a function of depth for a $Au/SrTiO_3/YBaCuO$ normal metal-dielectric-superconductor structure at 300K and 77K. The values for the normal metal layer are near those expected theoretically. The difference between the normal and superconducting states is substantial, as expected.

CONCLUSIONS

We have demonstrated the application of the confocal resonator technique to vertical profiling problems on a number of interesting structure types. Those shown here include implanted semiconductors and various conductor/dielectric multilayer structures. Vertical resolution on the scale of tens of nanometers have been demonstrated in a completely non-invasive and quick measurement procedure. The technique is applicable to a variety of materials and carrier concentrations. It is therefore of potential interest for a wide range of technologies for the purpose of analysis or monitoring of the materials or processes using those materials.

REFERENCES

[1] G. D. Boyd and J. P. Gordon, "Confocal multimode resonator for millimeter through optical wavelength masers," Bell Sys. Tech. Jour., vol. 40, pp.489-508, Mar. 1961.

[2] J. S. Martens, V. M. Hietala, D. S. Ginley, T. E. Zipperian and G. K. G. Hohenwarter, "Confocal resonators for measuring the surface resistance of high temperature superconducting films," Appl. Phys. Lett., vol. 58, pp. 2543-2545, Jun. 1991.

[3] K. E. Lonngren, J. W. Mink, and J. B. Beyer, "On the focused Fabry-Perot resonator in plasma diagnostics," IEEE Trans. on MTT, vol. MTT-12, pp. 548-549, Sept. 1964.

[4] V. M. Hietala, J. S. Martens, C. P. Tigges, T. A. Plut, B. F. Cole and R. S. Withers, "Surface resistance imaging of high temperature superconducting materials," presented at the 1992 Fall MRS meeting, Boston, MA, 30 Nov. 1992.

[5] R. E. Collin, Foundations for Microwave Engineering, McGraw-Hill, New York, 1966, pp. 237-254.

[6] D. M. Pozar, Microwave Engineering, Addison-Wesley, New York, 1990, chp. 6.

[7] C. B. Yarling, W. H. Johnson, W. A. Keenan, and L. A. Larson, "Uniformity mapping in ion implantation," Solid State Tech., vol. 21, pp. 57-61, Dec. 1991.

[8] T. Van Duzer and C. W. Turner, Principles of Superconductive Devices and Circuits, Elsevier, New York, 1981, chp. 3.